ISSN 0036-0236, Russian Journal of Inorganic Chemistry, 2011, Vol. 56, No. 5, pp. 759–770. © Pleiades Publishing, Ltd., 2011.

PHYSICAL METHODS OF INVESTIGATION

Synthesis, Spectroscopic, Electrochemical, DNA Binding and Photocleavage Studies on Coordination Compounds of Bis(4-aminophenyl)methane Based Novel Schiff Bases[1]

N. Raman and A. Selvan

Research Department of Chemistry, VHNSN College, Virudhunagar-626 001, India

e-mail: drn_raman@yahoo.co.in

Received September 15, 2009

Abstract—Two novel Schiff bases, 4,4'-methylenedianilidene-bis(3-methoxy-4-hydroxy-benzaldehyde) (L_1) and 4,4'-methylenedianilidene-bis(3,4-dimethoxybenzaldehyde) (L_2), have been prepared by condensing 4,4'-methylenedianiline (MDA) with vanillin and 3,4-dimethoxybenzaldehyde (DMB) respectively in ethanolic medium. Metal complexes of the above Schiff bases are prepared from salts of Cu(II), Zn(II), Co(II) and VO(IV). They are characterized by elemental analysis, molar conductivity, magnetic moment measurements, IR, ^{1}H NMR, UV-Vis., FAB Mass, and EPR spectra. The elemental analysis data exhibit the formation of 1 : 1 [M : L] ratio. The mode of bonding and the geometry of the complexes have been confirmed on the basis of IR, UV-Vis. and magnetic moment measurements. These data reveal a square-planar geometry for all the complexes except VO(IV) which has square-pyramidal geometry. The molar conductance measurements of the Schiff base complexes reveal the existence of non-electrolytic nature. The interactions of complexes with calf thymus DNA (CT-DNA) have been investigated by electronic absorption spectroscopy, viscosity measurements and cyclic voltammetry. The results indicate that the complex can bind to DNA by intercalation modes. The Schiff bases and their metal complexes have been evaluated for their antifungal and antibacterial activities against different species of pathogenic fungi and bacteria and their results are compared with standard drugs.

DOI: 10.1134/S0036023611050202

1. INTRODUCTION

Schiff bases have been widely used as bidentate ligands in the field of coordination chemistry [1–3] They are important class of ligands due to their synthetic flexibility, selectivity and sensitivity towards the central metal atom, structural similarities with natural biological substances and also due to the presence of imine group (N=CH–) which imports in elucidating the mechanism of transformation and racemization reactions in biological system [4]. They are found useful in catalysis, in medicine as antibiotics and anti-inflammatory agents and in the industry as anticorrosion agents [5–7]. Recently, Schiff base complexes have been widely investigated for their properties and applications in different fields, such as catalysis and materials chemistry [8, 9]. For example, metal complexes possess distinct second-order nonlinear optical [9] and fluorescent [10] properties that are closely related to the coordinated metal centre.

4,4'-Methylenedianiline (MDA), known as Bis(4-aminophenyl)methane, is used as intermediate in the manufacture of polyurethane foams. It is also used as a curing agent for epoxy resins, urethane elastomers, a corrosion preventative for iron, antioxidant for lubricating oils, rubber processing and preparation of azo-dyes [11]. It is a hazardous substance that causes liver damage, skin and eye irritation [12]. On the other hand, it was reported that some Schiff bases of aniline derivatives display anti-inflammatory and antipyretic properties [13, 14]. The complexes were found to be active against some microorganisms. It induces gene mutations in bacteria. In mammalian cell cultures, MDA is an inducer of chromosomal aberrations in the presence of an exogenous metabolisation system.

Transition metal complexes that are suitable for binding and cleaving double-stranded DNA are of considerable current interest due to their various applications in nucleic acid chemistry like foot-printing and sequence-specific binding agents, for modeling the restriction enzymes in genomic research, and as structural probes for therapeutic applications in cancer treatment [15]. Cleavage of DNA can be achieved by targeting its basic constituents like base and/or sugar by an oxidative pathway or by hydrolysis of phosphoester linkages. Complexes showing photo-induced cleavage of DNA have significant advantage over their "chemical nuclease" analogues in the absence of any other reagents like a reducing species and/or H_2O_2 for their activity. Besides, compounds cleaving DNA on photo-activation usually are known

[1] The article is published in the original.

to show localized effects in therapeutic applications and are non-toxic in the absence of light [16]. These facts tempted us to synthesize metal complexes involving MDA. Hence, we herein carried out an attempt to investigate the complexes involving MDA, having NN donor type to evaluate the biological activities like antibacterial, antifungal, DNA cleavage and biding studies.

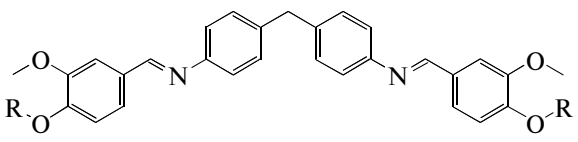

Scheme 1. Chemical diagram of the Schiff base ligand
R = H (4,4'-methylenedianilidene-bis(3-methoxy-4-hydroxybenzaldehyde);
R = CH_3 (4,4'-methylenedianilidene-bis(3,4-dimethoxybenzaldehyde).

2. EXPERIMENTAL

2.1. Materials and Methods

All the chemicals used were of reagent grade (Aldrich) and of highest purity. The elemental analyses were performed using a Perkin-Elmer CHN 2400 elemental analyzer. Metal analyses were carried out complexometrically [17]. IR spectra were recorded using KBr discs on a Perkin-Elmer 1430 spectrophotometer. ^{1}H NMR and ^{13}C NMR spectra (300 MHz) of the samples were recorded in $CDCl_3$ by employing TMS as internal standard on a Bruker Avance DRX 300 FT-NMR spectrometer. Fast atomic bombardment mass spectra (FAB-MS) were obtained using a VGZAB-HS spectrometer in a 3-nitrobenzylalcohol matrix. The X-band ESR spectra of the complexes were recorded at RT (300 K) and LNT (77 K) using TCNE (tetracyanoethylene) as the g-marker. The electronic spectra of the complexes in UV-Vis. region were recorded in DMF solution using Shimadzu model 1601 UV-Vis. spectrophotometer. Electrochemical studies were recorded in DMF solution using a glassy carbon working electrode and $[NBu_4]ClO_4$ was used as supporting electrolyte. Room temperature magnetic susceptibility measurements were carried out on a modified Gouy-type magnetic balance, Hertz SG8-5HJ. The molar conductivity was measured for the complexes (10^{-3} M) in DMF solution using a conductometer model 601/602.

2.2. Synthesis of Schiff Bases and Their Complexes

Schiff bases were prepared by the addition of 4,4'-methylenedianiline (1.98 g, 10 mmol) to 3-methoxy-4-hydroxybenzaldehyde (3.04 g, 20 mmol) (L_1) /3,4-dimethoxybenzaldehyde (3.32 g, 20 mmol) (L_2) in 1 : 2 molar ratio in ethanol (50 mL). The reaction mixture was stirred in air at 60°C for 2 h. The precipitate formed was filtered off, washed with ethanol several times and dried in vacuum and stored in desiccator over $CaCl_2$. For L_1 (yellow product) the yield is 65% and for L_2 (pale yellow product) the yield is 75%.

The general structure of ligands obtained, from elemental analyses and spectral methods, is given in Scheme 1.

Cu(II), Co(II), Zn(II) and VO(IV) complexes of all ligands were prepared by the addition of a hot solution (60°C) of the appropriate metal chloride (0.001 mol) in an ethanol (25 mL) to the hot solution of the Schiff bases (0.466 g L_1 and 0.494 g L_2, 1 mmol) in the same solvent (25 mL). The resulting mixture was stirred under reflux for 3 h whereupon the complexes precipitated. The precipitates were filtered off, washed with ethanol and diethyl ether, dried in vacuum and stored in desiccator over $CaCl_2$.

2.3. Biological Activity

Antibacterial activity was done by the paper-disc plate method. The nutrient agar medium (peptone, NaCl, and agar-agar) and 5 mm diameter paper discs (Whatman number 1) were used. For antifungal study potato agar medium was used. The compounds were dissolved in DMF in different concentrations. The filter paper discs were soaked in different solutions of the compounds, dried, and then placed in the petri dishes previously seeded with the test organisms. The plates were incubated for 24–30 h at 28 ± 2°C and minimum inhibition concentration (MIC) was measured in each case, both antibacterial and the antifungal activities were calculated. The linear growth of the fungus was recorded by measuring the diameter of the fungus colony after 96 h.

3. RESULTS AND DISCUSSION

The synthesized novel Schiff base ligands, 4,4'-methylenedianilidene-bis(3-methoxy-4-hydroxybenzaldehyde and 4,4'-methylenedianilidene-bis(3,4-dimethoxybenzaldehyde) (Scheme 1) form stable complexes with Cu(II), Zn(II), Co(II) and VO(IV) metal ions. The analytical data of the complexes, together with their physical properties are given in Table 1. The Schiff base ligands behave as monobasic bidentate containing an NN coordination site. The analytical data of the complexes correspond to the general stoichiometry $[M(L)X_2]$, where M = Cu(II), Zn(II), Co(II) and VO(IV), L = ligand ($C_{29}H_{26}N_2O_4$) (L_1)/($C_{31}H_{30}N_2O_4$) (L_2) and X = Cl. The value of molar conductance of complexes in DMF indicates that the complexes are non-electrolytes. The molecu-

Table 1. Physical characterization, analytical, molar conductance, and magnetic susceptibility data of the ligands and their complexes

Compound	Colour	mp (°C)	Yield (%)	Found (Calcd.) (%)				Molar conductance λ_m (ohm^{-1} cm^2 mol^{-1})	μ_{eff} (BM)
				M	C	H	N		
L_1									
$[C_{29}H_{26}N_2O_4]$	Yellow	77	65	–	74.45 (74.62)	5.48 (5.60)	5.96 (5.98)	–	–
$[CuC_{29}H_{26}N_2O_4Cl_2]$	Black	>250	50	10.52 (10.55)	57.89 (57.92)	4.32 (4.35)	4.58 (4.63)	1.39	1.73
$[CoC_{29}H_{26}N_2O_4Cl_2]$	Light yellow	101	42	9.81 (9.85)	58.40 (58.41)	4.29 (4.34)	4.64 (4.69)	3.26	2.6
$[ZnC_{29}H_{26}N_2O_4Cl_2]$	Pale yellow	>250	70	10.79 (10.83)	57.68 (57.76)	4.28 (4.34)	4.63 (4.64)	1.78	–
$[VOC_{29}H_{26}N_2O_4Cl_2]$	Pale green	>250	58	7.39 (8.42)	57.62 (57.63)	4.27 (4.32)	4.59 (4.62)	2.54	1.71
L_2									
$[C_{31}H_{30}N_2O_4]$	Pale yellow	144	75	–	75.24 (75.26)	6.07 (6.08)	5.62 (5.65)	–	–
$[CuC_{31}H_{30}N_2O_4Cl_2]$	Dark brown	193	52	10.07 (10.09)	59.11 (59.14)	4.79 (4.80)	4.41 (4.45)	1.42	1.69
$[CoC_{31}H_{30}N_2O_4Cl_2]$	Brown	112	55	9.39 (9.41)	59.58 (59.62)	4.78 (4.81)	4.42 (4.47)	3.34	2.9
$[ZnC_{31}H_{30}N_2O_4Cl_2]$	Pale yellow	163	65	10.32 (10.34)	58.94 (59.00)	4.71 (4.75)	4.38 (4.43)	1.69	–
$[VOC_{31}H_{30}N_2O_4Cl_2]$	Dark green	>250	80	7.98 (8.02)	58.79 (58.87)	4.74 (4.76)	4.39 (4.43)	2.48	1.75

lar weight results are in broad agreement with the conductance data suggesting monomeric formulations.

3.1. Mass Spectral Studies

The mass spectra of the ligands and their metal complexes were recorded and compared for their stoichiometric composition. In the present investigation, the mass spectrum of L_1 shows the formation of molecular ion peak M^+ at m/z = 466, the total molecular weight of the ligand, corresponding to $[C_{29}H_{26}N_2O_4]^+$ ion. This is supported by the "Nitrogen Rule", since the compound possesses two nitrogen atoms. Further, the spectrum exhibits the fragments at m/z 15, 17, 31, 123, 150, and 166 corresponding to $[CH_3]^+$, $[OH]^+$, $[OCH_3]^+$, $[C_7H_7O_2]^+$, $[C_8H_8NO_2]^+$, and $[C_{13}H_{10}]^+$, respectively. The FAB mass spectrum of copper complex of L_1 shows the molecular ion peak M^+ at m/z = 600 which confirms the stoichiometry of metal complexes as being of the ML type. In the complex one of the fragment ions exhibits a peak at 530 m/z suggesting the presence of two chloride ions. This was further supported by the mass spectra of other complexes. The observed peaks were in good agreement with their empirical formulae, as indicated from microanalytical data. Thus, the mass spectral data reinforced the conclusion drawn from the analytical and conductance values.

3.2. IR Spectra and Mode of Bonding

The IR spectra of the complexes were compared with those of the free ligands in order to determine the coordination sites that may be involved in chelation. There were some guide peaks in the spectra of the ligands, which were helpful in achieving this goal. The position and/or the intensities of these peaks are expected to change upon chelation. The spectra of the ligands show a band at 1606 cm^{-1} for L_1 and 1542 cm^{-1} for L_2 respectively which are assigned to $\gamma_{(C=N)}$ of azomethine group [18, 19]. They are bathochromic shifted to 1600 and 1513 cm^{-1} on complexation, indicative of the involvement of N donor atom of C=N group in coordination to the metal ions [20]. The complexes show a new medium intensity band in the region 525 cm^{-1} which is due to the formation of M–N bond [21]. The weak band observed at 325–340 cm^{-1} is probably due to the formation of the M–Cl bond [22]. In addition to other bands, the vanadyl complexes show an additional strong band at 940–960 cm^{-1} attributed to V=O frequency.

3.3. Electronic Spectra

The electronic spectra of the complexes were recorded in DMF. In the spectrum of the ligand, the band at 26737 cm^{-1} nm range is assigned to the $n \longrightarrow \pi^*$ transition of the azomethine group. During the formation of the complexes, this band is shifted to

Table 2. Electronic absorption spectral data of the ligands and their compounds

Compounds	Solvent	Absorption (cm^{-1})	Band assignment	Geometry
L_1				
$[C_{29}H_{26}N_2O_4]$	EtOH	26737	INCT*	–
		34602	INCT	
$[CuC_{29}H_{26}N_2O_4Cl_2]$	DMF	13605	$^2A_{1g}(F) \longrightarrow B_{1g}(P)$	Square-planar
		28089	INCT	
		33003	INCT	
$[CoC_{29}H_{26}N_2O_4Cl_2]$	DMF	16447	$^1A_{1g} \longrightarrow {}^1B_{1g}$	Square-planar
		27100	INCT	
		30487	INCT	
$[VOC_{29}H_{26}N_2O_4Cl_2]$	DMF	11641	$^2B_2 \longrightarrow {}^2E$	Square-pyramidal
		13831	$^2B_2 \rightarrow {}^2A_1$	
		27027	INCT	
		33112	INCT	
L_2				
$[C_{31}H_{30}N_2O_4]$	CH_3CN	25839	INCT	–
		37735	INCT	
$[CuC_{31}H_{30}N_2O_4Cl_2]$	DMF	17730	$^2A_{1g}(F) \longrightarrow {}^2B_{1g}(P)$	Square-planar
		32573	INCT	
		43668	INCT	
$[CoC_{31}H_{30}N_2O_4Cl_2]$	DMF	16366	$^1A_{1g} \longrightarrow {}^1B_{1g}$	Square-planar
		25906	INCT	
		38022	INCT	
$[VOC_{31}H_{30}N_2O_4Cl_2]$	DMF	12755	$^2B_2 \longrightarrow {}^2E$	Square-pyramidal
		17793	$^2B_2 \longrightarrow {}^2A_1$	
		23529	INCT	
		37593	INCT	

Note: * INCT–intraligand charge transfer band.

lower wavelength, suggesting that the nitrogen atom of the azomethine group is coordinated to the metal ion. Another intense band in higher energy region of the spectra of the free ligand was related to $\pi \longrightarrow \pi^*$ transition of benzene rings [23]. Based on the data obtained (Table 2), a square-planar geometry has been assigned to the complexes except VO(IV) complex which has square-pyramidal geometry. These values are comparable with other reported complexes [24].

The spectrum of Cu(II) complexes of L_1 and L_2 showed absorption bands at 13605 and 17730 cm^{-1} respectively, which could be attributed to the $^2A_{1g}(F) \longrightarrow {}^2B_{1g}(P)$ transition characterized Cu(II) ion in a square-planar geometry [25]. The square-planar geometry is achieved by the coordination of one molecule of ligand, which acting as a monobasic bidentate ligand, to the copper (II) ion [25].

The electronic spectra of the vanadyl complexes of L_1/L_2 display four bands (Table 2) in the region of 11641/12755 cm^{-1}, 13831/17793 cm^{-1}, 27027/23529 cm^{-1}, and 23529/37593 cm^{-1}. The first two bands are assigned to spin-allowed transitions $^2B_2 \longrightarrow {}^2E$ and $^2B_2 \longrightarrow {}^2A_1$ and the other two are INCT bands respectively. The position of these bands indicates that the complexes have five coordinated square-pyramidal geometries.

The electronic spectra of Co(II) complexes of L_1/L_2 recorded were very similar to each other and the bands in the region 16447/16366 cm^{-1} assigned to the $^1A_{1g} \longrightarrow {}^1B_{1g}$ transition which clearly indicate the square-planar geometry of the complexes (Table 2).

3.4. NMR Spectral Studies

The ^1H NMR spectra of the synthesized ligands and their compounds were recorded in $CDCl_3$ and DMSO-d_6 solution, using tetramethylsilane (TMS) as internal standard. All the protons in the spectra were identified, and the total number of calculated protons is in good agreement with the proposed structure. The spectra showed two signals at chemical shifts 9.80–9.90 and 3.91–4.13 ppm range for the protons of the phenolic-OH and the OCH_3 groups, respectively. The singlet peak in the 8.07–8.59 ppm range corresponds to the proton attached to the CH=N group in L_1 clearly indicates that the magnetic environment is equivalent for all such protons, suggesting the pres-

Table 3. The spin Hamiltonian parameters and bonding parameters of VO(IV) complex in DMSO at 300 and 77 K

Complex	Hyperfine constant $\times 10^{-4}$ cm^{-1}			G tensors			α^2	β^2	γ^2	$K_\parallel$	$K_\perp$	γ_{av}
	$A_\parallel$	$A_\wedge$	A_{iso}	$\gamma_\parallel$	$\gamma_\perp$	γ_{iso}						
$[VOL_2Cl_2]$	167	59	99.3	1.91	1.98	1.87	1.01	1.08	1.04	1.09	1.05	1.96

ence of a planar ligand in these complexes [26]. However, Zn(II) complex of corresponding ligand exhibited such signals are slightly shifted upon complexation which confirming the absence of CH=N proton upon complexation. A multiplet was observed at 7.0–7.6 ppm for the aromatic protons. A multiplet in the region 3.44–3.51 ppm may be assigned to the methylene protons (–C–CH_2–C–, 2H) of the condensed aldehyde moiety. The results obtained are quite comparable with the reported data [27].

The mode of bonding suggested above has also been confirmed by the ^{13}C NMR spectral data. The ^{13}C NMR spectra of the zinc complex show the expected number and positions of signals. The number of signals of sharp peaks represent the number of carbons of the compound which are chemically non-equivalent. The resonance of the carbon attached to the hydroxyl and methoxy groups in the ligand is observed at δ 159.3 and δ 151.92 respectively. The ^{13}C NMR spectrum of L_1 exhibits signals at δ 55.96 (–OCH_3), δ 120.96, 124.27, 129.60, 138.63, and 141.28 (5CH), δ 149.43, 150.27, 151.92 (3C), δ 110.44 (=CH), and δ 40.92 (–CH_2–) characteristic resonance lines with the corresponding chemical shifts. The azomethine (C=N) carbon is downward on complexation, and a signal appears in the δ 108.88–106.40 range. This shielding provides support that the azomethine nitrogen involves in the complexation [28].

3.5. Electronic Paramagnetic Spectra

The X-band EPR spectra of oxovanadium(IV) (d^1, ^{51}V, I = 7/2) complex resolved at room temperature to exhibit all the eight-hyperfine lines on X band at frequency of 9.1 GHz under the magnetic-field strength of 3000 G. The calculated values of $g_\parallel$, $g_\perp$, g_{av}, for oxovanadium(IV) complex are given in Table 3. Here, $g_{av} = 1/3[2g_\perp + g_\parallel]$. The g tensor values of this oxovanadium(IV) complex can be used to derive the ground state. From the observed values, it is clear that $g_\perp > g_\parallel > 2$ suggesting that the complex has square pyramidal geometry [29] with the unpaired electron in the d_{xy} orbital of the metal. The lowering of g value than the free electron value g_e is due to the spin orbit interaction of the ground state d_{xy} with low lying excited state as evident from the value of the exchange interaction term G, estimated from the expression

$$G = (g_\parallel - 2)/(g_\perp - 2),$$

which measures the exchange interaction between the metal centres in a polycrystalline solid, has been calculated. According to Hathaway [30] if G > 4, the exchange interaction is negligible, but G < 4 indicates considerable exchange interaction in the solid complexes. The present vanadyl complex, the G value is greater than 4 which indicates that the exchange interaction is negligible. They are also inconsistent with any other ion, clearly indicating that a non-exchangeable vanadium(IV) ion is present in this sample.

The in-plane σ-bonding covalence parameter (α^2), out-of-plane σ-bonding (γ^2) and in-plane σ-bonding (β^2) parameters are calculated using simple M.O theory. If the α^2 value = 0.5, it indicates complete covalent bonding, while the value of $\beta^2 = 1.0$ suggests complete ionic bonding. The observed value of α^2 (1.01) indicates that the complex has some ionic character. This is also confirmed by orbital reduction factors which give significant information about the nature of bonding in the oxovanadium(IV) complex, derived from the relative magnitudes of $K_\parallel$ and $K_\perp$. In the case of pure σ-bonding $K_\parallel \approx K_\perp = 0.77$, whereas $K_\parallel < K_\perp$ implies considerable in-plane π-bonding while for out-of-plane π-bonding $K_\parallel > K_\perp$. For the present complex, the observed order is $K_\parallel$ (1.09) > $K_\perp$ (1.05) implying a greater contribution from out-of-plane π-bonding than from in-plane π-bonding in metal-ligand π-bonding.

3.6. Screening of Antibacterial and Antifungal Activities

The antimicrobial screening data are presented in Tables 4 and 5. The Table shows that the metal complexes exhibit antimicrobial properties and it is important to note that the synthesized complexes exhibit enhanced activity in contrast to the free ligands. It has been suggested that the ligands with the N-donor systems might have inhibited enzyme production, since enzymes that require free hydroxy groups for their activity appeared to the especially susceptible to deactivation by the ions of the complexes. The variation in the effectiveness of the different compounds against different organisms depends on their impermeability of the microbial cells or on the difference in the ribosome of the microbial cells [31]. The hydrocarbon acts as a lipophilic group to drive the compound through the semi permeable membrane of the cell. The increased lipophilic character of these complexes seems to be responsible for their enhanced potent antibacterial activity. Chelation reduces the polarity of

Table 4. Minimum inhibition concentration of the synthesized compounds against growth of six bacteria (mg/mL)

Compound	*S. typhi*	*S. aureus*	*B. subtilis*	*E. coli*	*P. putita*	*K. pneumoniae*
L_1 ($C_{29}H_{26}N_2O_4$)	60	70	75	80	70	65
$CuC_{29}H_{26}N_2O_4Cl_2$	23	25	18	29	34	29
$CoC_{29}H_{26}N_2O_4Cl_2$	35	45	25	38	30	35
$ZnC_{29}H_{26}N_2O_4Cl_2$	21	19	15	21	25	23
$VOC_{29}H_{26}N_2O_4Cl_2$	45	55	34	48	50	56
L_2 ($C_{31}H_{30}N_2O_4$)	65	75	60	85	85	60
$CuC_{31}H_{30}N_2O_4Cl_2$	22	34	28	30	31	25
$CoC_{31}H_{30}N_2O_4Cl_2$	39	45	34	36	45	27
$ZnC_{31}H_{30}N_2O_4Cl_2$	20	24	19	25	29	23
$VOC_{31}H_{30}N_2O_4Cl_2$	35	48	55	44	55	52
Streptomycin	18	12	10	14	18	12

Note: *S. typhi*–*Salmonella typhi, S. aureus*–*Staphylococcus aureus, B. subtilis*–*Bacillus subtilis, E. coli*–*Escherichia coli, P. putida*–*Pseudomonas putida, K. pneumoniae*–*Klebsiella pneumoniae*.

Table 5. Minimum inhibition concentration of the synthesized compounds against growth of five fungi (mg/mL)

Compound	*A. niger*	*A. flavus*	*R. stolonifer*	*C. albicans*	*R. bataicola*
L_1 ($C_{29}H_{26}N_2O_4$)	75	80	85	70	65
$CuC_{29}H_{26}N_2O_4Cl_2$	24	36	37	25	28
$CoC_{29}H_{26}N_2O_4Cl_2$	35	48	40	24	31
$ZnC_{29}H_{26}N_2O_4Cl_2$	19	25	35	22	25
$VOC_{29}H_{26}N_2O_4Cl_2$	45	52	55	32	37
L_2 ($C_{31}H_{30}N_2O_4$)	65	52	45	55	20
$CuC_{31}H_{30}N_2O_4Cl_2$	16	28	35	37	46
$CoC_{31}H_{30}N_2O_4Cl_2$	25	30	40	42	48
$ZnC_{31}H_{30}N_2O_4Cl_2$	15	25	28	35	30
$VOC_{31}H_{30}N_2O_4Cl_2$	38	32	41	45	40
Nystatin	10	8	16	12	14

Note: *A. niger*–*Aspergillus niger, A. flavus*–*Aspergillus flavus, R. stolonifer*–*Rhizopus stolonifer, C. albicans*–*Candida albicans, R. bataicola*–*Rhizoctonia bataicola*.

the central ion mainly because of the partial sharing of its positive charge with the donor groups and possible π-electron delocalization within the whole chelate ring. This chelation increases the lipophilic nature of the central metal atom, which favors its permeation through the lipid layer of the membrane and blocking the metal binding sites on enzymes of microorganism [26]. The results revealed that the ligand has no promising activity against the bacteria and fungai used, the decreasing microbial activities of zinc > copper > cobalt > vanadyl complexes, exhibit excellent activity against all types of the microorganisms used. The antifungal activity of the complexes was evaluated by the agar plate techniques by mixing solutions of the metal complexes in different concentrations in DMF which were then mixed with the medium.

3.7. Chemical Nuclease Activity

The extent of supercoiled (SC) pUC19 DNA cleavage to its nicked circular (NC) form was monitored by agarose gel electrophoresis. The oxidative cleavage of DNA in the presence of a reducing agent, mercaptopropionic acid (MPA, 5 mM) has been studied by gel electrophoresis using supercoiled (SC) pUC19 DNA (0.5 μg) in 50 mM Tris-HCl/50 mM NaCl buffer (14 μL, pH 7.2) treated with the complexes (50 μM in 2 μL DMF) (Fig. 1). Bands were visualized by UV light and photographed to determine

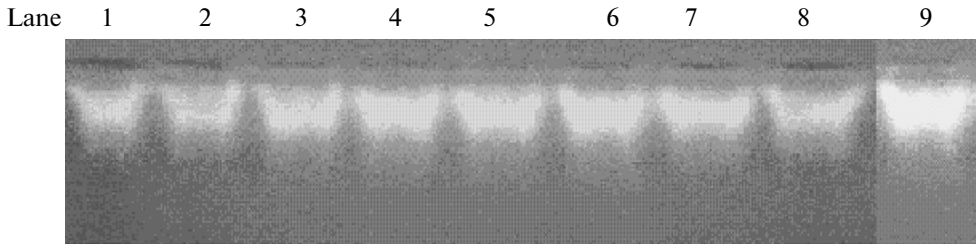

Fig. 1. Gel electrophoresis diagram showing UV light-induced DNA (SC pUC19, 0.5 μg) cleavage activity of complexes 2–9 (50 μM) at 365 nm (12 W) with exposure time of 5 min. Lane 1, DNA control; lane 2, DNA + $[CuL_1Cl_2]$ + MPA; lane 3, DNA + $[CuL_2Cl_2]$ + MPA; lane 4, DNA + $[CoL_1Cl_2]$ + MPA; lane 5, DNA + $[CoL_2Cl_2]$ + MPA; lane 6, DNA + $[VOL_1Cl_2]$ + MPA; lane 7, DNA + $[VOL_2Cl_2]$ + MPA; lane 8, DNA + $[ZnL_1Cl_2]$ + MPA; lane 9, DNA + $[ZnL_2Cl_2]$ + MPA.

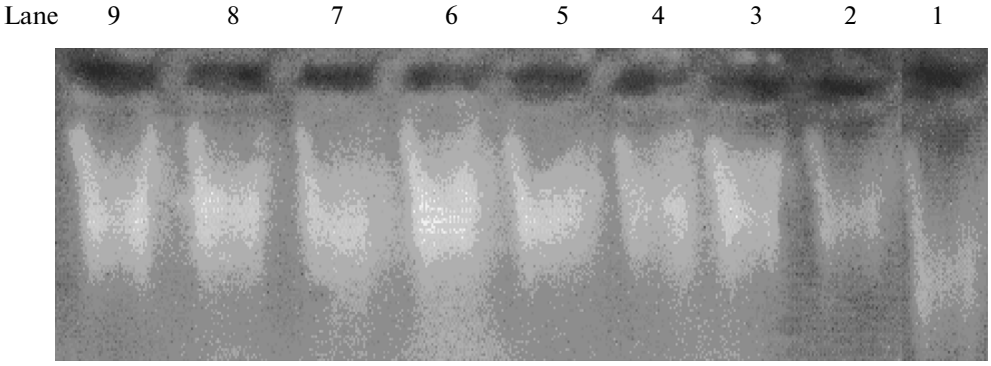

Fig. 2. Gel diagram showing the photo-cleavage of SC pUC19 DNA (0.5 μg) by 1–9 (50 μM) in DMF-Tris buffer medium on 1 h exposure at 365 nm. Lane 1, DNA control; lane 2, DNA + $[CuL_1Cl_2]$; lane 3, DNA + $[CuL_2Cl_2]$; lane 4, DNA + DMSO (4 μL) + $[CuL_1Cl_2]$; lane 5, DNA + DMSO (4 μL) + $[CuL_2Cl_2]$; lane 6, DNA + NaN_3 (90 μM) + $[CuL_1Cl_2]$; lane 7, DNA + NaN_3 (90 μM) + $[CuL_2Cl_2]$; lane 8, DNA + D_2O (14 μL) + $[CuL_1Cl_2]$; lane 9, DNA + D_2O (14 μL) + $[CuL_2Cl_2]$.

the extent of DNA cleavage from the intensities of the bands using UVITEC Gel Documentation System. Control experiments using MPA alone shows small significant cleavage of SC DNA when compared to complexes even on longer exposure time. All the synthesized complexes cleave the DNA from its SC to NC form even in the absence of inhibitors on irradiation with UV light at 365 nm.

3.7.1. DNA Photocleavage Activity

For photo-induced DNA cleavage studies, the reactions were carried out under illuminated conditions using UV light of 365 nm (Fig. 2). After exposure to the light, each sample was incubated for 1 h at 37°C in the dark and analyzed using gel electrophoresis. The inhibition reactions were carried out by adding reagents (DMSO, 4 μL; sodium azide, 90 μM) prior to the addition of the complexes. The samples after incubation were added to the loading buffer containing 25% bromophenol blue, 30% glycerol (3 μL) and the solution was finally loaded on 0.8% agarose gel containing 1.0 μg mL^{-1} ethidium bromide. Electrophoresis was carried out in a dark chamber for 2 h at 60 V in TAE (Trisacetate EDTA) buffer. Bands were visualized by UV light and photographed. To test the possibility that photo induced cleavage involves the formation of singlet oxygen, which is known to react with guanine residues at neutral pH, [32] the cleavage was tested in the presence of D_2O. Singlet oxygen would be expected to induce more strand scissions in D_2O than in H_2O due to its longer lifetime in the former solvent. Due corrections were made for the low level of nicked circular (NC) form present in the original supercoiled (SC) DNA sample and for the low affinity of EB binding to SC compared to its NC form. The results indicate the important role of metal in these photo-induced DNA cleavage reactions. The complexes show the presence of a charge-transfer band range 325–380 nm. It is likely that the photo-cleavage at 365 nm involves photo excitation of the charge-transfer band leading to the formation of an excited singlet state that through the triplet state activates molecular oxygen to form reactive singlet oxygen species. Moreover, we will show that this cleavage can be induced by metal complexes known to bind in different manners to DNA. In addition, control experiments were carried out in order to investigate the effect of oxygen in aerobic condition and the possibility of that DNA cleavage occurred via a hydroxyl radical-based mechanism. Experimental

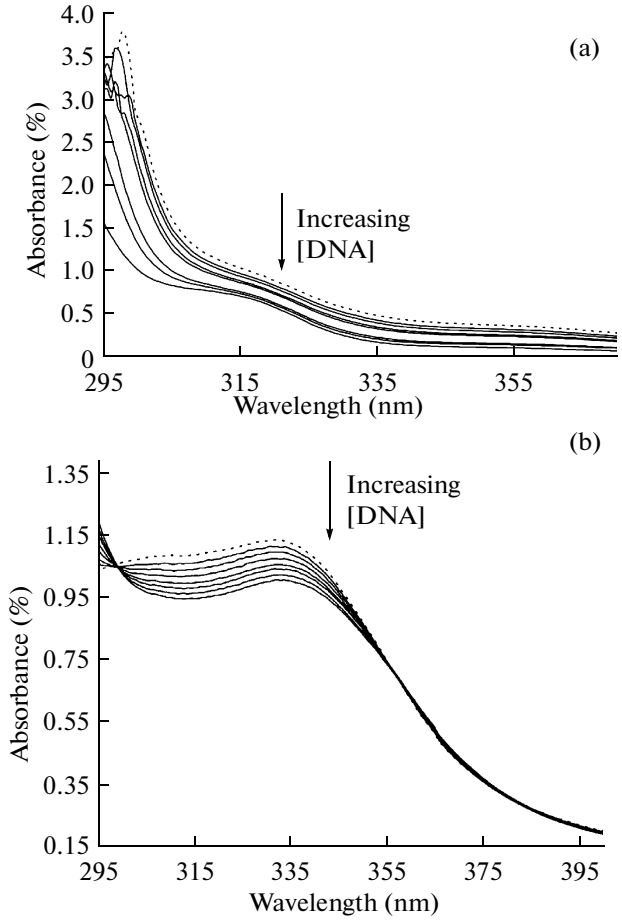

Fig. 3. (a) Absorption spectra of $[CuL_1Cl_2]^{2+}$ in the absence and presence of CT-DNA in Tris-HCl buffer. The absorbance changes upon increasing CT-DNA concentrations. [Cu] = (10 μM), [DNA] = (0–90 μM), the arrows show the decrease in intensity upon increasing DNA concentration. (b) Absorption spectra of $[CuL_2Cl_2]^{2+}$ in the absence and presence of CT-DNA in Tris-HCl buffer. The absorbance changes upon increasing CT-DNA concentrations. [Cu] = (10 μM), [DNA] = (0–90 μM), the arrows show the decrease in intensity upon increasing DNA concentration.

results showed that the cleavage was not influenced by addition of radical scavenger such as 4 mol/L DMSO, and NaN_3, whereas, the oxidative degradation of DNA by $Fe(EDTA)^{2-}/H_2O_2$ was almost totally inhibited by those radical scavenges at ten times lower concentration [33]. Control experiments show that hydroxyl radical scavenger DMSO inhibits the cleavage. The singlet oxygen quencher sodium azide does not show any inhibition.

4. DNA BINDING STUDIES

The interaction of metal complex with DNA can occur through three types of binding modes viz., intercalation, outside binding in the groove and outside binding with self-stacking along the DNA surface. Absorption spectroscopy is one of the convenient tools for examining the interaction between ligands and nucleic acids. The different modes of interaction of a metal complex with DNA can be studied not only by this technique but also cyclic voltammetry (CV) and differential pulse voltammetry (DPV) were employed to probe the binding of metal complexes to DNA in solution. DPV data were used to obtain quantitative information about the interaction of these metal complexes with CT-DNA. The difference between forward and backward peak potentials can provide a rough evaluation of the degree of the reversibility of one electron transfer reaction. The analysis of cyclic voltammetry responses with the scan rate varying 50 to 250 mV/s gives the evidence for a quasi-reversible one electron oxidation. The ratio of cathodic to anodic peak height was less than one. However, the peak current increases with the increase of the square root of the scan rate. The $Ip/v^{1/2}$ value is almost constant for all scan rates. This establishes the electrode process as diffusion controlled [34].

4.1. Absorption Spectral Studies

The interaction of the complex with DNA was investigated using absorption spectra. The absorption spectra of complex in the absence and presence of CT-DNA (at a constant concentration of the complex) was studied. As the concentration of DNA increases, the MLCT transition bands of the complexes exhibit hypochromism. Based on the observations of complexes, we presume that there are some interactions between complexes and DNA. An intercalative binding of a complex to DNA generally results in hypochromism along with a blue shift (hypochromism shift) of the electronic spectral band [35]. The absorption spectra of Cu(II) complexes of L_1 and L_2 in the absence and presence of CT-DNA at a constant concentration of complex [Cu] = 10 μM is shown in Figs. 3a and 3b. To quantitatively determine the binding strength of the complexes, the intrinsic binding constant K_b of the complexes with CT-DNA was obtained by monitoring the changes in absorbance of the complexes with increasing DNA concentrations according to Eq. (1):

$$[DNA]/(\varepsilon_a - \varepsilon_f) = [DNA]/(\varepsilon_b - \varepsilon_f) + 1/(K_b(\varepsilon_b - \varepsilon_f)), \quad (1)$$

where [DNA] is the concentration of DNA in nucleotides, and ε_a, ε_f and ε_b are the extinction coefficients of the apparent, free, and bound metal complexes, respectively. The hypochromism and blue-shifts observed above which may suggest an intercalative mode. On plotting $[DNA]/(\varepsilon_a - \varepsilon_f)$ vs. [DNA], K_b is determined from the ratio of the slope to the intercept. The intrinsic binding constant K_b obtained for the synthesized complexes approximately is in the range $1.59–9.35 \times 10^5$ (Table 6).

Table 6. Absorption spectral properties of synthesized complexes with DNA

Complexes	λmax		Δλ (nm)	Hypochromicity (%)	$K_b \times 10^5$ (M^{-1})
	Free	Bound			
$[CuL_1Cl_2]$	321.5	315	6.5	12.04	9.35
$[CoL_1Cl_2]$	371.5	369.5	2.0	1.78	8.50
$[VOL_1Cl_2]$	428	437.5	9.5	35.6	1.59
$[CuL_2Cl_2]$	342	338.5	3.5	3.09	4.93
$[CoL_2Cl_2]$	379.5	378	1.5	2.02	2.58
$[VOL_2Cl_2]$	377.5	376	1.5	1.21	4.07

Table 7. Electrochemical parameters for the interaction of DNA with synthesized complexes

Complexes	Redox couple	E_{pc} (V)		I_{pc} (μA)		$E_{1/2}$ (V)		ΔE_p		K^+/K^{2+}
		Free	Bound	Free	Bound	Free	Bound	Free	Bound	
$[CuL_1Cl_2]$	Cu(II)/Cu(I)	0.218	0.289	4.14	3.83	0.429	0.453	0.423	0.329	0.06
	Cu(III)/Cu(II)	0.104	0.147	4.57	2.57	0.343	0.390	0.478	0.487	0.18
$[CuL_2Cl_2]$	Cu(II)/Cu(I)	−0.655	−0.681	9.68	7.91	−0.412	−0.397	0.486	0.568	2.75
$[CoL_1Cl_2]$	Co(II)/Co(I)	−0.721	−0.667	1.25	1.14	−0.443	−0.44	0.556	0.454	0.12
	Co(III)/Co(II)	0.163	0.211	2.19	1.98	0.392	0.469	0.458	0.576	0.15
$[CoL_2Cl_2]$	Co(II)/Co(I)	−0.672	−0.696	6.91	6.28	−0.524	−0.517	0.295	0.358	2.54
$[ZnL_1Cl_2]$	Zn(II)/Zn(I)	−0.684	−0.615	9.44	4.97	−0.548	−0.566	0.272	0.097	0.07
$[ZnL_2Cl_2]$	Zn(II)/Zn(I)	0.188	0.237	4.20	2.01	0.480	0.535	0.585	0.596	0.15
$[VOL_1Cl_2]$	VO(II)/VO(I)	−0.569	−0.522	9.52	6.99	−0.176	−0.161	0.353	0.323	0.16
$[VOL_2Cl_2]$	VO(II)/VO(III)	0.621	0.672	1.25	1.04	0.77	0.816	0.298	0.289	0.13
	VO(II)/VO(I)	−0.605	−0.626	7.59	7.46	−0.445	−0.412	0.32	0.427	2.26

4.2. Electrochemistry

Electrochemical properties of the complexes were studied on a Pt disc electrode in dimethylformamide containing 0.05 M n-Bu_4NClO_4 as the supporting electrolyte. Table 7 summarizes the electrode potentials for all complexes in DMF in the absence and presence CT-DNA in Tris-HCl buffer (pH 7.2). All the measurements were carried out in 10^{-3} M solutions in the potential range +1.2 to −1.2 with scan rate 50 mV s^{-1}, glass-carbon electrode as a working electrode, platinum wire as an auxiliary electrode and Ag/AgCl as a reference electrode at room temperature.

The drop of the voltammetry currents in the presence of DNA may be attributed to slow diffusion of the metal complex bound to CT DNA. This in turn indicates the extent of binding affinity of the complex to DNA. The net shift in $E_{1/2}$ can be used to estimate the ratio of equilibrium constants for the binding of the 3+ and 2+ ions to DNA.

$$\begin{array}{ccccc} M^{3+} + \mathbf{e}^- & \rightleftharpoons & M^{2+} & & E_f^0 \\ K^{3+}\uparrow\downarrow & & K^{2+}\uparrow\downarrow & & \\ M^{3+}\text{–DNA} + \mathbf{e}^- & \rightleftharpoons & M^{2+}\text{–DNA} & & E_b^0 \end{array}$$

Scheme 2.

Scheme 2 represents a Nernstian electron transfer to a system in which both the oxidized and reduced forms are associated with a third species in solution (DNA). In this scheme M^{3+} and M^{2+} represent the oxidized and reduced forms of the metal complex. E_f^0 and E_b^0 are the formal potentials of the 3+/2+ couple, in the free and bound forms respectively. K^{3+} and K^{2+} are the corresponding equilibrium constants for binding of the 3+ and 2+ species to DNA. The Nernst equation for the reversible redox reactions of the free and bound species and the corresponding equilibrium constants for binding of each oxidation state to DNA for a one electron redox process are given as follows:

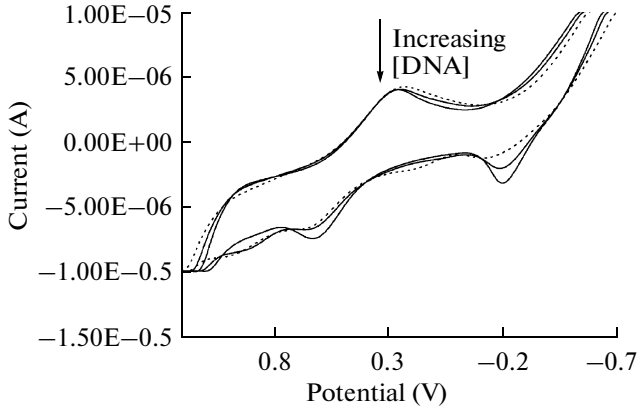

Fig. 4. Cyclic voltammogram of $[CuL_1Cl_2]$ (0.25 mM) in the absence (dash line) and in the presence (dark line) of CT-DNA.

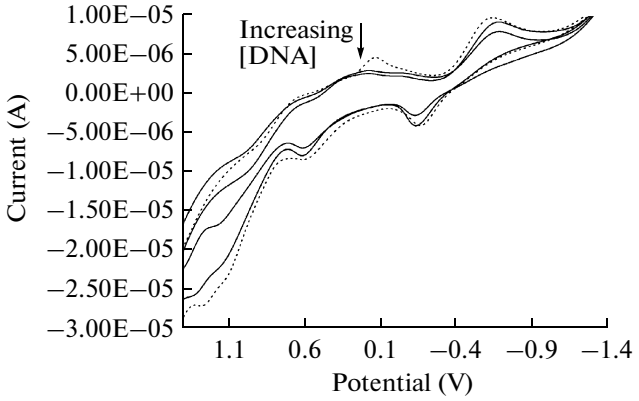

Fig. 5. Cyclic voltammogram of $[CuL_2Cl_2]$ (0.25 mM) in the absence (dash line) and in the presence (dark line) of CT-DNA.

$$E_b^0 - E_f^0 = 0.0591 \log(K_{red}/K_{ox}).$$

The cyclic voltammogram of CuL_1 exhibited quasi–reversible one electron redox process involving the Cu(II)/Cu(I) couple with cathodic peak at E_{pc} = 0.218 V and oxidation peak E_{pa} = 0.641 V (Fig. 4). For this couple, the difference between cathodic and anodic peak potential ΔE_p and the ratio of anodic and cathodic peak currents I_{pa}/I_{pc} are less than unity. The formal electrode potential $E_{1/2}$ taken as an average of E_{pc} and E_{pa} was 0.429 V in the absence of DNA. Addition of CT-DNA to CuL_1 results in significant reduction in cathodic and anodic peak current due to slow diffusion of an equilibrium mixture of the free and DNA-bound complex to the electrode surface [36]. The observed shift in $E_{1/2}$ values to less negative potentials suggests that Cu(II) and Cu(I) forms of CuL_1 bind to DNA. During the incremental addition of CT-DNA to the complex, one additional anodic peak is appeared at –0.187 V and no reduction peak in the absence and presence of DNA. In the absence of DNA, Cu(II) complex of L_2 shows two redox couples. The first redox couple cathodic peak appears at 0.104 V for Cu(III)/Cu(II) (Fig. 5) (E_{pa} = 0.582 V, E_{pc} = 0.104 V, ΔE_p = 0.478 V, $E_{1/2}$ = 0.343 V) and second redox couple cathodic peak appears at –0.655 for Cu(II)/Cu(I) (E_{pa} = –0.169 V, E_{pc} = –0.655 V, ΔE_p = 0.486 V, $E_{1/2}$ = –0.412 V). The ratio of i_{pc}/i_{pa} is less than unity. The change in current upon DNA addition can be used to quantify the binding of CuL_2 to DNA. The above electrochemical experimental results indicate that preferential stabilization of Cu(I) form over Cu(II) form on binding to DNA.

In the absence of CT-DNA, the redox couple cathodic peak appears at 0.163 V for Co(III)/Co(II) (E_{pa} = 0.621 V, E_{pc} = 0.163 V, ΔE_p = 0.458 V, $E_{1/2}$ = 0.392 V) and second redox couple cathodic peak appears at –0.672 for Co(II)/Co(I) (E_{pa} = –0.377 V, E_{pc} = –0.672 V, ΔE_p = 0.295 V, $E_{1/2}$ = –0.524 V). The ratio of i_{pc}/i_{pa} is less than unity. This indicates that the reaction of the complex on Pt electrode surface is quasi-reversible redox process. The incremental addition of CT-DNA to the complex causes a negative shift in $E_{1/2}$ of 77 V and a decrease in ΔE_p of 58 V. The i_{pc}/i_{pa} values also decrease in the presence of DNA. The decrease of the cathodic and anodic peak currents of the complex in the presence of DNA is due to the decrease in the apparent diffusion coefficient of the cobalt(III) complex upon complexation with DNA. The ratio of the binding constants K^+/K^{2+} for DNA binding of Co(II)/Co(I) complex of L_2 is calculated and found to be greater than unity. This indicates that the binding of Co(II) complex to DNA is small compared to that of the Co(I) complex. In the absence of CT-DNA, the redox couple cathodic peak appears at –0.721 V for cobalt complex of L_1. This redox couple ratio of i_{pc}/i_{pa} is less than unity. This indicates that the reaction of the complex on working electrode surface is quasi-reversible redox process. In addition, the peak potentials, E_{pa}, E_{pc}, and $E_{1/2}$ have a shift to more negative potential. The changes of peak current and shift of potential are observed in the complex upon addition of CT-DNA.

The electrochemical parameters of other synthesized Zn(II) and VO(IV) complexes of L_1 and L_2 are shown in Table 7. The shift of the redox potential of the complexes in the presence of DNA to more negative values indicates a binding interaction between the complex and DNA that makes the complexes less readily reducible. The drop of the voltammetry currents in the presence of CT-DNA can be attributed to diffusion of the metal complex bound to the large, slowly diffusing DNA molecule. The decreased extents of the peak currents observed for the complexes upon addition of CT-DNA may indicate that complexes interact with DNA through intercalating way.

Differential pulse voltammogram (DPV) of the $[CuL_1]^{2+}$ complex both in the presence and absence of DNA is given in Fig. 6. The peak potential and current of the $[CuL_1]^{2+}$ are changed in the presence of K^{2+}/K^+

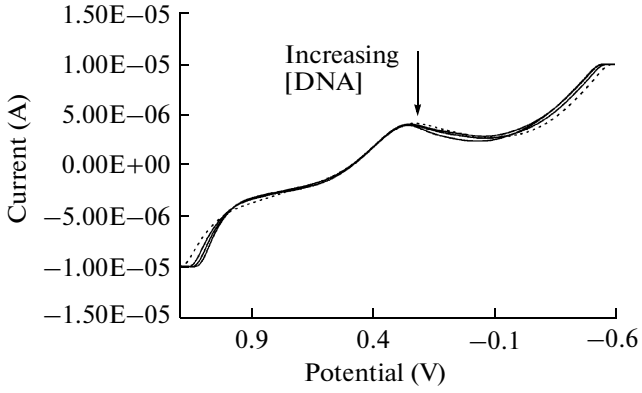

Fig. 6. Differential pulse voltammogram of $[CuL_1Cl_2]^{2+}$ in the absence (dash line) and presence (dark line) of different concentration of DNA.

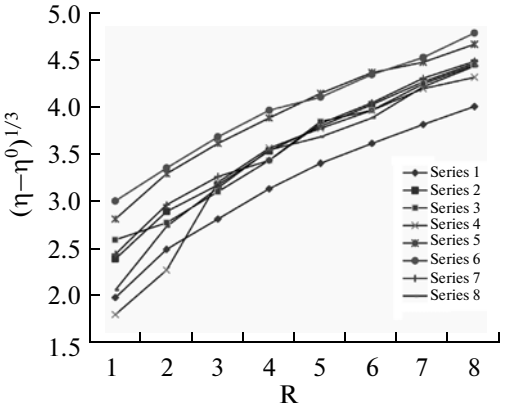

Fig. 7. The effect of increasing of $[CuL_1Cl_2]$, $[CoL_1Cl_2]$, $[ZnL_1Cl_2]$, $[VOL_1Cl_2]$, $[CuL_2Cl_2]$, $[CoL_2Cl_2]$, $[ZnL_2Cl_2]$, and $[VOL_2Cl_2]$, on the relative viscosity of calf thymus DNA are series 1–8 respectively at 25.0°C.

value for the copper complex is less than unity suggesting preferential stabilization of Cu(I) form over Cu(II) form on binding to DNA. The possible mechanism is shown below:

$$\begin{array}{ccc} CuL^{2+} + e^- & \rightleftharpoons & CuL^+ \qquad E_f^0 \\ K^{2+} \uparrow\downarrow & & \uparrow\downarrow K^+ \\ CuL^{2+}\text{–DNA} + e^- & \rightleftharpoons & CuL^+\text{–DNA} \qquad E_b^0 \end{array}$$

DPV of the complexes as a function of added DNA also indicates a large decrease in current intensity with a small shift in formal potential due to the intercalative interaction of complexes.

4.3. Viscosity Studies

To further clarify the nature of the interaction between the complex and DNA was carried out by viscosity measurements. Viscosity experiments give valuable information regarding mode of binding metal complex with DNA. A classical intercalative mode demands that the DNA helix must lengthen as base pairs are separated to accommodate the binding ligand, leading to the increase of DNA viscosity [37]. When a metal complex intercalates between the base pairs of DNA, length of DNA increases which leads to the increase in viscosity. On the other hand, a partial and/or non-classical intercalation of the ligand with the DNA helix reduces its effective length and concomitantly its viscosity. The plots of relative specific viscosities Vs [complex]/[DNA] are shown in Fig. 7. All the metal complexes change the relative viscosity of DNA in a manner consistent with binding by intercalation mode and the effect of the complexes on the viscosity of rod-like DNA is shown in Fig. 7. On the basis of the viscosity results, it clearly shows that the compounds can intercalate between adjacent DNA base pairs causing an extension in the helix, and thus increase the viscosity of DNA and that complexes bind with DNA through intercalation mode leading to the greater increase in viscosity of the DNA with an increasing concentration of complex [38].

CONCLUSIONS

The results of this study clearly indicate that the present Schiff bases act as bidentate ligands coordinating the metal ion through azomethine nitrogen. The analytical data show the presence of one metal ion per ligand molecule and suggest a mononuclear structure for the complexes. Magnetic and electronic spectra reveal that the complexes of these ligands can exist in square-planar geometry for Cu(II), Co(II), and Zn(II) except VO(IV) which has square-pyramidal geometry. The binding behavior of complexes with DNA has been characterized by absorption titration, cyclic voltammetry and viscosity measurements. These three methods indicate that the complexes may intercalate into DNA. The antimicrobial data suggest that the complexes have more activity than free ligands.

ACKNOWLEDGMENTS

The authors express their sincere thanks to the Managing Board, Principal and Head of the Department of Chemistry, VHNSN College, Virudhunagar. The authors are thankful to SAIF, CDRI Lucknow for microanalysis, IR and FAB mass spectral analysis.

REFERENCES

1. C. Sousa, C. Freire, and B. de Castro, Molecules. **8**, 894 (2003).
2. L. T. Yildirm and O. Atakol, Cryst. Res. Technol. **37**, 1352 (2002).
3. A. Pui, Croat. Chem. Acta **75**, 165 (2002).
4. C. Spinu and A. Kriza, Acta Chim. Slov. **47**, 179 (2000).

5. J. Liu, B. Wu, B. Zhang, and Y. Liu, Turk J. Chem. **30**, 41 (2006).
6. A. Budakoti, M. Abid, and A. Azam, Eur. J. Med. Chem. **41** (1), 63 (2006).
7. V. X. Jin, S. J. Tan, and J. D. Ranford, Inorg. Chim. Acta **358** (3), 677 (2005).
8. M. J. Sabater, M. Alvaro, H. Garcia, et al., J. Am. Chem. Soc. **123**, 7074 (2001).
9. S. Di Bella, Chem. Soc. Rev. **30**, 355 (2001).
10. K. E. Splan, A. M. Massari, G. A. Morris, et al., Eur. J. Inorg. Chem. 2348 (2003).
11. *The Merck Index. An Encyclopedia of Chemicals, Drugs and Biologicals*, 1th ed., Ed. by S. Budavari (Merck, Rahway, New York, 1989).
12. S. S. Que Hee, *Proceedings of International Conference on Occupational and Environmental Exposure Skin to Chemicals, Hilton Crystal City, 2002*, p. 1.
13. R. N. Patel, V. L. N. Gundla, and D. K. Patel, Indian J. Chem. A **47**, 353 (2008).
14. J. M. Takacs, D. S. Reddy, S. A. Moteki, et al., J. Am. Chem. Soc. **126**, 4494 (2004).
15. M. J. Wilkinson, P. W. N. M. van Leeuwen, and J. N. H. Reek, Org. Biomol. Chem. **32**, 2371 (2005).
16. H. Ali and J. E. VanLier, Chem. Rev. **99**, 2379 (1999).
17. T. Premkumar and S. Govindarajan, J. Therm. Anal. Cal. **84**, 395 (2006).
18. H. M. El-Tabl, F. A. El-Saied, and M. I. Ayad, Synth. React. Inorg. Met.-Org. Chem. **32**, 1247(2002).
19. R. Olar, M. Badea, E. Cristurean, et al., J. Therm. Anal. Cal. **80**, 451 (2005).
20. A. A Osowole, G. A. Kolawole, and O. E. Fagade, Int. J. Chem. **15** (4), 237 (2005).
21. D. M. Boghaei and S. Mohebi, J. Chem. Res. **6**, 660 (2001).
22. D. Kulkarni, A. Patil, and S. Badami, Int. J. Electrochem. Soc. **4**, 717 (2009).
23. E. Conpolat and M. Kaya, J. Coord. Chem. **57** (14), 1217 (2004).
24. D. U. Warad, C. D. Satish, V. H. Kulkarini, and C. S. Bjgur, Indian J. Chem. A **39**, 415 (2000).
25. B. N Figgs, *Introduction to Ligand Field* (Wiley, New York, 1966).
26. N. Padmapriya, S. Arunachalam, A. Manimaran, et al., Spectrochim. Acta A **72**, 670 (2009).
27. A. Golcu, M. Turner, H. Demirelli, and R. A. Wheatley, Inorg. Chim. Acta **358**, 1785(2005).
28. J. Lewinski, I. Justyniak, J. Zachara, and E. Tratkiewicz, Organometallics **22**, 4151 (2003).
29. Jagdish Prasad, Prem Yadav, Ved Prakash, and Krishna Srivastava, J. Indian Chem. Soc. **84**, 650 (2007).
30. *Essays in Chemistry*, Ed. by B. J. Hathaway, J. N. Bardley, and R. D. Gillard (Academic Press, New York, 1971).
31. S. Rich and J. G. Horsfall, Phytopathology **42**, 457 (1952).
32. P. C. Lee and M. A. Rodgers, J. Photochem. Photobiol. (1986).
33. R. P. Hertzberg and P. B. Dervan, Biochemistry **23**, 3934 (1984).
34. *Electrochemical Methods: Fundamentals and Applications*, Ed. by A. J. Bard and L. R. Izatt, 2nd ed. (Wiley, New York/London, 2001).
35. A. Tysoe, R. J. Morgan, A .D. Baker, and T. C. Strekas, J. Phys. Chem. **97**, 1707 (1993).
36. J. Liu, T. Lu, T. Zhang, et al., J. Inorg. Biochem. **91**, 269 (2002).
37. S. Satyanarayana, J.C. Dabroniak, and J. B. Chaires, Biochemistry **31**, 9319 (1992).
38. M. Chauhan, K. Banerjee, and F. Arjmand, Inorg. Chem. **46**, 3072 (2007).